Journal of Solid State Chemistry **163,** 491–497 (2002)
doi:10.1006/jssc.2001.9435, available online at http://www.idealibrary.com on IDEAL®

Structural Characterization of Doped Calcium Tartrate Tetrahydrate

Manuel E. Torres,* Trinidad López,* Josefina Stockel,* Xavier Solans,†,[1] Maite García-Vallés,† Enrique Rodríguez-Castellón,‡ and Cristina González-Silgo§

*Dep. Física Básica, Universidad de La Laguna, E-38204, La Laguna, Spain; †Dep. Cristallografia, Universitat de Barcelona, E-08028 Barcelona, Spain; ‡Dep. Química Inorgánica, Universidad de Málaga, E-29071, Málaga, Spain; and §Dep. Física Fundamental II, Universidad de La Laguna, E-38204, La Laguna, Spain

Received June 5, 2001; in revised form October 10, 2001; accepted October 26, 2001

Crystals of calcium tartrate tetrahydrate were grown in silica gel medium in pure form and with barium, strontium, cobalt, nickel, manganese, zinc, and cadmium as dopants. The crystals, with formula $D_xCa_{1-x}(C_4H_4O_6).4H_2O$ (where D = doping atom), were characterized by X-ray diffraction, photoelectron spectroscopy, and Raman spectroscopy. Some of the doping atoms are located in the host lattice and others are distributed at random positions, especially on the surface of the crystals. In the host lattice the doping atom replaces Ca when an earth alkaline atoms is used but occupies an interstitial site when a transition metal atom is used. The dielectric permittivity is higher in doped compounds. © 2002 Elsevier Science (USA)

INTRODUCTION

Considerable attention has been devoted to tartrate salts owing to their electrical properties. Some of them are ferroelectric and/or piezoelectric compounds, which are used in transducers and many linear and nonlinear mechanical devices. Recent research has examined the calorimetric and electric behavior of rubidium hydrogen tartrate (1) and ammonium tartrate (2) crystals. The phase transition mechanism of sodium potassium (Rochelle salt) (3) and sodium ammonium tartrate (4) has recently been reviewed.

We examine the relationship between the dielectric properties of tartrate salts with divalent cations and their crystal structure. The thermal and electromagnetic behaviors of manganese (5) and zinc tartrate (6) were previously investigated. Here we studied tetrahydrated calcium tartrate, $[CaC_4H_4O_6 \cdot 2H_2O] \cdot 2H_2O$. These crystals were grown with divalent cations as doping atoms in order to modify their structure. The divalent cations used were Ba, Sr, Zn, Cd, Co, Mn, and Ni. The structure of tetrahydrated calcium tartrate is known (7). This compound shows the nonpolar space group $P2_12_12_1$, which is opposite to the ferroelectricity established in (8). The structure of transition metal tartrates is also known. This family of compounds crystallizes with a different number of water molecules and belongs to two noncentrosymmetric space groups. For instance, MnT (9) and CuT (10) belong to the polar group $P2_1$, and ZnT (11) and CdT (12) belong to $P2_12_12_1$. The latter undergoes a structural phase transition before the water is lost (13). Earth alkaline tartrates show different 3D packing (not dimeric). Barium tartrate crystallizes in the $P2_12_12_1$ space group with nine oxygen atoms from six different tartrates around the cation and without water molecules (14). The strontium cation is eight-coordinated and crystallizes in the polar space group $P2_1$ (15). We measured the dopant concentration on tetrahydrate calcium tartrate and analyzed the structural and electric variations due to the doping.

EXPERIMENTAL SECTION

Crystal Growth

Crystals of calcium tartrate tetrahydrate were grown in silica gel medium in pure form and with different doping atoms. A 1 M solution of sodium metasilicate was added to another of 1 M tartaric acid L (+) until pH 4.5. Once that gelled, a 1 M aqueous solution of $CaCl_2$ was poured on top and allowed to diffuse into the gel. Calcium tartrate tetrahydrate crystals grew in the gel. To grow the doped crystals, an aqueous solution of the chloride of the dopant was used together with the outer reactant $CaCl_2$. The molar ratio used for mixing $CaCl_2$ and dopant chloride was 0.05 and the experimental temperature was 313 K. Some of the single crystals show an octahedral shape with an apical distance of around 2 mm and an equatorial distance of around 2.5 mm.

Techniques for Determination of Composition and Molecular and Crystal Structure

The crystals were analyzed by X-ray powder diffraction with a Siemens D500 diffractometer, using Cu$K\alpha$ radiation

[1] To whom correspondence should be addressed.

0022-4596/02 $35.00

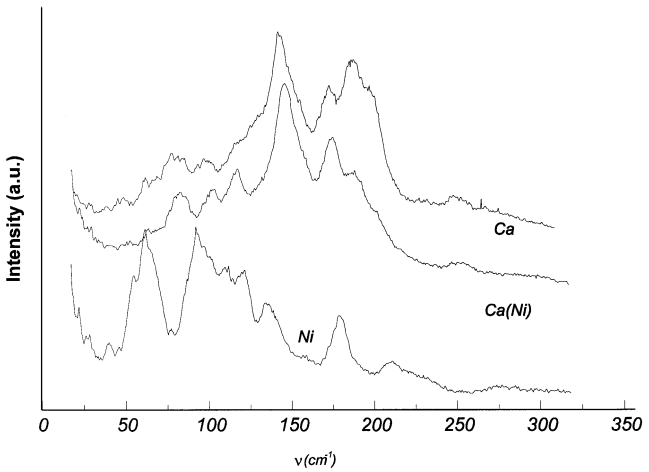

FIG. 1. The rotatory and translatory external modes and the longitudinal acoustic mode first member (LAM-1) of pure calcium tartrate tetrahydrate [Ca], Ni-doped calcium tartrate tetrahydrate [Ca(Ni)], and pure nickel tartrate pentahydrate.

and a secondary monochromator. The step size was 0.05°, the time of each step 10 sec, and the 2θ range was 10–80°.

The doping concentration was analyzed by induced condensed plasma (ICP) with a Jobin-Yvon analyzer and surface analysis by X-ray photoelectron spectroscopy (XPS) on single crystals. The XPS equipment used was a Physical Electronics 5700 X-ray spectrometer with two excitation sources (Mg$K\alpha$, $hv = 1253.6$ eV and Al $K\alpha$, $hv = 1486.6$ eV) and a multichannel electronic analyzer 80-365.

Raman spectra were excited on the powder sample using a Jobin-Yvon T64000 spectrometer, and an argon ion laser excitation. The detector used was a Control Data CDC. The spectra were recorded with the 514.5-nm line and a light power equal to 1.05 W. All spectra were calibrated against selected neon lines. The position, half-width, and relative intensity of each peak was determined, assuming it to be a Lorentzian function (the Gaussian contribution is negligible).

TABLE 1
Molar Fraction Determined Using Different Compositional Analysis Techniques

Doping ion	Single crystal by DRX	Average value from several crystals by ICP	Surface analysis by XPS
Ba^{2+}	0.002	0.003	0.005
Sr^{2+}	0.011	0.025	0.084
Co^{2+}	0.005	0.008	0.119
Ni^{2+}	0.038	0.04	0.048
Mn^{2+}	0.03	0.04	0.047
Cd^{2+}	0.024	0.020	0.018
Zn^{2+}	0.02–0.03	0.025	0.005

The crystal structure of calcium L-tartrate tetrahydrate doped with Ba, Sr, Cd, Ni, Zn, Mn, and Co was determined. Two samples of Zn-doped crystal were measured, because morphological differences were observed between the two samples. This was done in order to measure two sets of intensity data with a different molar fraction of the doping atom. A similar method was followed in all single-crystal structure determinations. Diffraction data were collected on an Enraf-Nonius CAD4 automated diffractometer equipped with a graphite monochromator. The ω–2θ scan technique was used to record the intensities. Scan widths were calculated as $A + B \tan \theta$, where A is estimated from the mosaicity of the crystal and B allows for the increase in peak width due to Mo$K\alpha_1$–$K\alpha_2$ splitting. The unit cell parameters were obtained by a least-squares fit to the automatically centered settings from 25 reflections ($12° < 2\theta < 21°$). The intensities from three control reflections for each measurement showed no significant fluctuation during the data collection. Empirical absorption corrections were made via ϕ scans (16). Attempts to obtain spherical crystal failed because the crystals were too fragile. The structures were solved by direct methods, using the SHELXS computer program (17), and refined by the full-matrix least-squares method, using the SHELXL computer program

TABLE 2
Crystal Data and Structure Refinement (x in Molar Fraction)

	x	Color	a (Å)	b (Å)	c (Å)	Volume (Å^3)	S (F^2)	$R1$	w$R2$
(Ca)	0	White	9.215(2)	9.631(2)	10.573(3)				
(Ca, Zn)	0.020(5)	White	9.167(9)	9.545(8)	10.501(7)	918.8(13)	1.11	0.047	0.11
(Ca, Zn*)	0.029(5)	White	9.148(11)	9.530(5)	10.503(8)	915.7(14)	1.14	0.049	0.11
(Ca, Ni)	0.038(5)	Pale green	9.157(3)	9.558(10)	10.475(7)	916.8(12)	1.15	0.044	0.10
Ca, Co)	0.005(2)	Pink	9.2210(10)	9.626(2)	10.568(2)	938.0(3)	1.44	0.035	0.12
(Ca, Mn)	0.03(1)	Pale pink	9.126(11)	9.560(5)	10.509(8)	916.9(14)	2.14	0.122	0.26
(Ca, Cd)	0.024(5)	White	9.136(9)	9.546(5)	10.482(7)	914.2(12)	1.10	0.048	0.12
(Ca, Sr)	0.005(1)	White	9.082(17)	9.529(5)	10.463(5)	905.5(18)	1.09	0.037	0.11
(Ca, Ba)	0.002(1)	White	9.078(17)	9.535(5)	10.456(11)	905(2)	1.11	0.038	0.11

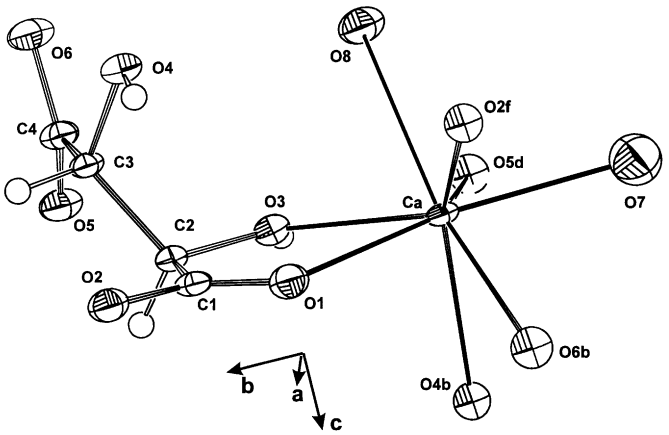

FIG. 2. View of Ca coordination polyhedron showing the numbering of atoms.

(18). The function minimized was $w||F_o|^2 - |F_c|^2|^2$, where the weighting scheme was $w = [\sigma^2(I) + (k_1P)^2 + k_2P]^{-1}$ and $P = (|F_o|^2 + 2|F_c|^2)/3$. The values of k_1 and k_2 were also refined. The chirality of the structure was defined from the Flack coefficient (19).

Dielectric Permittivity Measurements

Dielectric permittivity measurements were carried out using a Hewlett-Packard impedance analyzer 4192A that was controlled by a microcomputer. Measurements were made at frequencies from 4×10^2 to 2×10^5 Hz with an applied voltage of 1 V_{pp} and over the temperature range $\sim$ 65–100°C. Pellet samples were compressed under a pressure of 300 MPa and a fine layer of silver paint was used as electrode. The pellet samples were then placed in the cell, which was enclosed in a resistance-heated furnace. The temperature of the sample was monitored using an iron constant thermocouple within an accuracy of $\pm$ 1°C. At each temperature, at least 25 min was allowed before measurements to ensure sample thermal equilibrium. The "pellet cell" description, sample preparation, and data collection were reported previously (20, 21). The dielectric permittivity ($\varepsilon^* = \varepsilon' - j\varepsilon''$) of the material was obtained when the input impedance of the cell was measured. $Y_e = j\omega[C_o + (\varepsilon' - j\varepsilon'')C_a]$ (22), where C_a is the geometric capacity of sample space and C_o is the residual capacity. Both parameters were calculated using standards.

DISCUSSION AND RESULTS

The formation of the doped crystals was corroborated with X-ray powder diffraction and Raman scattering. X-ray powder patterns show that the compounds are isostructural to calcium tartrate tetrahydrate with the peak positions displaced with those of pure compound and peaks of doped tartrate were not observed. Figure 1 shows, for example, the rotatory and translatory external modes and the longitudinal acoustic mode first member (LAM-1) ($\nu < 300$ cm^{-1}) of pure calcium tartrate tetrahydrate, nickel-doped calcium tartrate tetrahydrate, and pure nickel tartrate pentahydrate. These modes give information about the packing forces. Figure 1 shows that the nickel-doped calcium tartrate is not a mixture of two pure compounds while significant differences are observed in the external modes' intensities of

TABLE 3
Hydrogen Bond Lengths (in Å) for Selected Doped Crystals

	(Ca)	(Ca, Ba)	(Ca, Cd)	(Ca, Ni)	(Ca, Zn)	(Ca, Zn*)
O(3)–H(3)..O(10)	2.714(3)	2.686(6)	2.696(6)	2.702(5)	2.719(5)	2.692(5)
O(4)–H(4)..O(5)	3.132(2)					
O(4)–H(4)..O(6) (i)[a]	2.564(2)	2.536(5)	2.538(5)	2.550(4)	2.549(5)	2.550(4)
O(7)–H(7)..O(9)	2.765(3)	2.739(6)	2.747(6)	2.738(5)	2.756(6)	2.755(5)
O(7)–H(7A)..O(1) (ii)	2.875(3)	2.839(6)	2.853(6)	2.883(5)	2.870(6)	2.845(5)
O(8)–H(8)..O(10) (iii)	3.287(3)					
O(8)–H(8)..O(9) (iv)		3.253(7)	3.259(6)	3.273(5)	3.266(6)	3.252(5)
O(8)–H(8A)..O(4)	2.975(3)	2.938(6)	2.953(6)	2.963(5)	2.950(5)	2.943(5)
O(9)–H(9)..O(1) (v)	2.921(3)	2.882(6)	2.894(6)	2.876(5)	2.886(5)	2.904(5)
O(9)–H(9)..O(6) (vi)			3.241(6)		3.249(5)	
O(9)–H(9A)..O(5)	3.085(3)		3.061(6)	3.065(5)	3.069(5)	3.076(5)
O(9)–H(9A)..O(8) (vii)		3.253(7)				
O(10)–H(10)..O(5)		3.134(7)				3.148(5)
O(10)–H(10)..O(7) (vi)	3.019(3)		2.996(7)	2.949(6)	2.974(6)	2.997(6)
O(10)–H(10)..O(9) (viii)		3.476(8)				
O(10)–H(10A)..O(8) (ix)	3.149(3)			3.123(5)	3.137(6)	3.136(5)

[a]Symmetry codes: (i) $= \frac{1}{2} + x, \frac{1}{2} - y, -z$; (ii) $= 2 - x, -\frac{1}{2} + y, \frac{1}{2} - z$; (iii) $= \frac{3}{2} - x, -y, -\frac{1}{2} + z$; (iv) $= \frac{3}{2} - x, -1 - y, -\frac{1}{2} + z$; (v) $= -\frac{1}{2} + x, -\frac{1}{2} - y, 1 - z$; (vi) $= 1 - x, -\frac{1}{2} + y, \frac{1}{2} - z$; (vii) $= \frac{3}{2} - x, -1 - y, \frac{1}{2} + z$; (viii) $= x, 1 + y, z$; (ix) $= 1 - x, \frac{1}{2} + y, \frac{1}{2} - z$.

TABLE 4
Ca–O Bond Lengths (in Å) for the Different Doped Crystals

	Ca–O(1)	Ca–O(3)	Ca–O(7)	Ca–O(8)	Ca–O(4)b[a]	Ca–O(6)b	Ca–O(5)d	Ca–O(2)f
(Ca, Zn)	2.365(3)	2.458(3)	2.424(4)	2.475(4)	2.507(3)	2.406(4)	2.489(4)	2.404(4)
(Ca, Zn*)	2.353(3)	2.452(3)	2.418(4)	2.479(4)	2.503(3)	2.409(4)	2.487(4)	2.409(3)
(Ca, Ni)	2.376(3)	2.449(3)	2.428(4)	2.480(3)	2.483(3)	2.402(3)	2.473(3)	2.395(3)
(Ca, Co)	2.378(2)	2.469(3)	2.440(3)	2.485(3)	2.519(2)	2.419(3)	2.507(3)	2.431(3)
(Ca, Mn)	2.360(7)	2.450(7)	2.421(8)	2.482(7)	2.506(7)	2.405(7)	2.487(6)	2.411(7)
(Ca, Cd)	2.357(4)	2.456(4)	2.426(5)	2.469(4)	2.495(4)	2.404(4)	2.487(4)	2.405(4)
(Ca, Sr)	2.354(6)	2.447(6)	2.414(7)	2.468(7)	2.486(8)	2.397(7)	2.470(6)	2.388(7)
(Ca, Ba)	2.354(5)	2.448(5)	2.424(5)	2.466(5)	2.492(5)	2.392(5)	2.470(5)	2.394(5)
(Ca)	2.376(2)	2.468(2)	2.437(2)	2.488(2)	2.514(2)	2.423(2)	2.503(2)	2.424(2)

[a]Symmetry codes: b $= \frac{3}{2} - x, -y, \frac{1}{2} + z$; d $= 1 - x, -\frac{1}{2} + y, \frac{1}{2} - z$; f $= 2 - x, -\frac{1}{2} + y, \frac{1}{2} - z$.

116.2(2) [119.3(5) for pure Ca compound] and 188.9(3) [190.2(2)] cm^{-1}.

The composition (in molar fraction) of each selected crystal mounted on the automatic diffractometer was determined from structure refinement and by evaluating the electron density of the Ca site (Table 1). In the Sr- and Ba-doped crystals the doping atom was located in the same position as the Ca atom. The result with Sr is consistent with the isostructurality between Sr and Ca tartrate tetrahydrate (23). Ca and doping atoms were refined anisotropically with the same thermal coefficients, while in transition metal-doped crystals a defect of the electronic charge was found in the Ca site. Single-crystal X-ray diffraction, surface analysis using XPS, and ICP analysis all gave inconsistent results on the composition of the crystals. The concentration of doping on the surface was higher in Ba-, Sr-, and Co-doped calcium tartrate tetrahydrate and lower in the Zn-doped form. This could be explained by differences in solubility or the formation of surface impurities.

Crystal data and structure refinement results are listed in Table 2. This table shows that the cell volume decreases in the presence of doping ion. This may be attributable to different centering conditions in the two instruments; therefore, a crystal of calcium tartrate tetrahydrate was mounted on the diffractometer. The cell parameters of calcium tartrate tetrahydrate were $a = 9.213(5)$ Å, $b = 9.6126(9)$ Å, and $c = 10.555(3)$ Å. These are higher than those obtained in the crystals with doping ion. On the other hand the structure obtained for the pure crystal is similar to the originally solved structure. In the crystal structure determination process of doped crystals, Sr and Ba were located at the same site as the Ca ion, while the doping transition metal atoms were not located from a difference synthesis and a defect of the electronic charge was found in the Ca site. The crystal structure determination shows that the Ca atom is always eight-coordinated to six oxygen atoms (Fig. 2) which belong to four tartrate ions, O(1), O(3), O(2)f, O(4)b, O(6)b, and O(5)d (symmetry codes: f $= 2 - x, \quad y - \frac{1}{2}, \quad \frac{1}{2} - z$; b $= \frac{3}{2} - x, -y, \frac{1}{2} + z$; and d $= 1 - x, y - \frac{1}{2}, \frac{1}{2} - z$), and two

TABLE 5
Main Torsion Angles (in °)

	(Ca, Cd)	(Ca, Ni)	(Ca, Zn)	(Ca, Zn*)	(Ca, Mn)	(Ca, Co)	Ca
O(3)–Ca–O(1)–C(1)	− 7.8(3)	− 8.7(2)	− 8.1(3)	− 6.96(19)	− 6.7(7)	− 8.2(3)	− 7.7
O(7)–Ca–O(1)–C(1)	167.9(3)	170.3(2)	168.1(3)	168.1(2)	167.6(8)	167.7(3)	167.3
O(8)–Ca–O(1)–C(1)	62.0(3)	61.2(2)	61.8(3)	63.1(2)	63.1(7)	61.5(3)	61.9
O(6)b–Ca–O(1)–C(1)	− 151.0(3)	− 151.8(2)	− 151.5(3)	− 149.9(2)	− 149.9(8)	− 151.7(3)	− 151.1
O(7)–Ca–O(3)–C(2)	− 170.7(3)	− 172.9(2)	− 170.6(2)	− 170.20(17)	− 170.2(6)	− 170.8(2)	− 170.2
O(3)–Ca–O(6)b–C(4)b	61.0(4)	62.0(2)	59.7(3)	61.5(3)	62.5(8)	61.5(3)	61.3
O(1)–Ca–O(5)d–C(4)d	− 95.6(3)	− 94.5(3)	− 96.1(3)	− 96.0(2)	− 95.0(7)	− 95.2(3)	− 94.9
Ca–O(1)–C(1)–C(2)	8.4(5)	9.9(4)	8.6(4)	7.0(3)	6.9(11)	9.1(4)	8.4
Ca_e–O(5)–C(4)–O(6)	− 1.9(6)	− 3.2(4)	0.3(5)	− 2.0(4)	− 4.2(13)	− 2.2(5)	− 2.6
Ca_a–O(6)–C(4)–C(3)	4.1(5)	3.2(3)	5.9(4)	3.5(3)	2.6(11)	3.8(4)	4.1
O(3)–C(2)–C(3)–C(4)	58.9(4)	59.5(3)	57.6(3)	59.2(2)	58.6(9)	58.8(3)	58.7
O(4)–C(3)–C(4)–O(5)	157.3(3)	157.1(3)	158.3(3)	157.39(19)	156.2(7)	157.1(3)	156.6
O(4)–C(3)–C(4)–O(6)	− 26.3(5)	− 25.8(3)	− 27.6(4)	− 26.2(3)	− 25.3(10)	− 26.3(4)	− 26.6
C(2)–C(3)–C(4)–O(5)	31.8(5)	31.4(4)	33.3(4)	31.7(3)	31.2(11)	32.0(4)	31.8

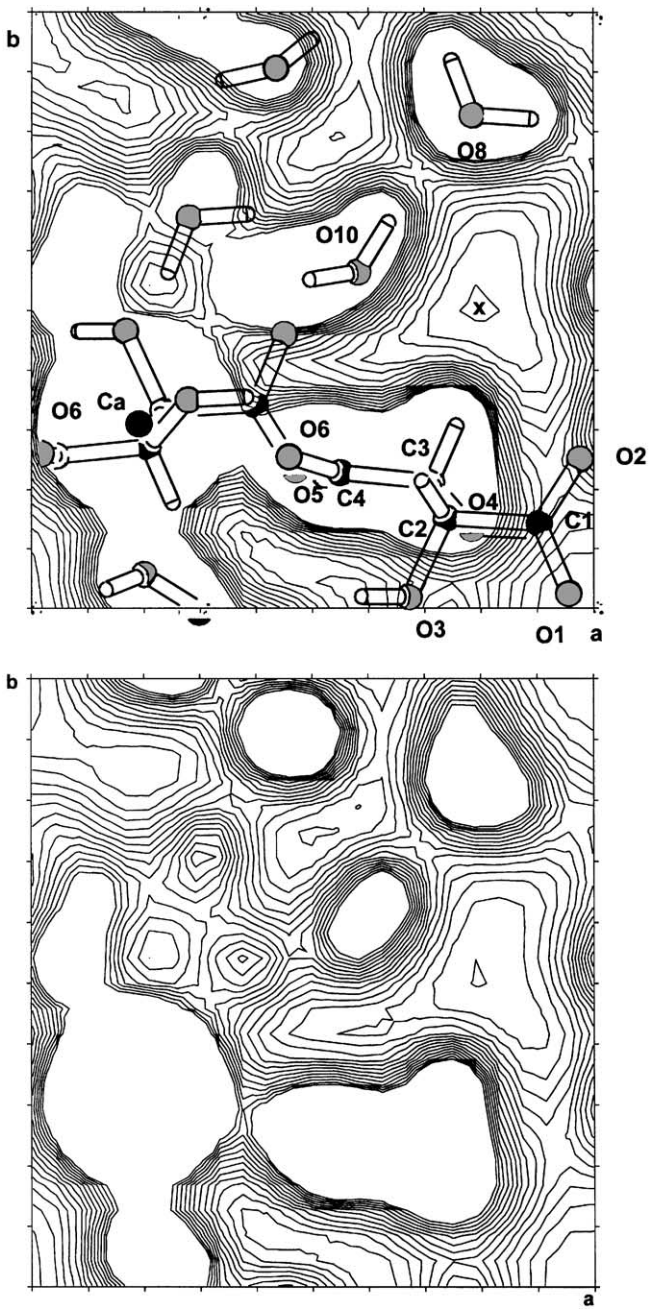

FIG. 3. Bond valence contour maps showing the interstitial site for Ni-doped calcium tartrate tetrahydrate (top) compared with the hole of pure calcium tartrate tetrahydrate (bottom). The highest valence contour level has been erased for clarity.

oxygen atoms from water molecules; O(7) and O(8), with the Ca–O bond parallel to the *b* and *c* axis, respectively. Each tartrate acts in hexadentate fashion being linked to four Ca ions. All structures consist of a 3D arrangement of tartrates, and the Ca–O bonds are practically parallel to different crystallographic axes. Thus Ca … O(2)f and Ca … O(5)d are parallel to the *a* axis, Ca … O(1) and Ca … O(3) parallel to the *b* axis, and Ca … O(4)b parallel to the *c* axis. In order to determine the differences between the different structures, a study using the half-normality plot (24, 25) was done. From the first plot, including all bond and nonbonded distances less than 4 Å, several hypotheses were examined until the "best" plot was reached, including the maximum distances possible, so as to give no trends of systematic errors. The distances excluded from this last plot were considered as the main differences between the structures. (The structure of pure calcium tartrate tetrahydrate was used as a reference in all comparisons.)

The main difference between the calcium L-tartrate tetrahydrate structure and the Ba- and Sr-doped crystal is in the localization of hydrogen atoms, which produces a different hydrogen bond scheme. In Table 3 the hydrogen bridges of the structure of the pure calcium tartrate tetrahydrate and the compound doped with Ba are presented (some of the hydrogens of the Sr-doped form were not located). Thus, while O(10) is hydrogen bonded to O(8) and O(7) atoms in the pure crystal, it is hydrogen bonded to O(5) and O(7) in the doped compounds. These variations could explain the

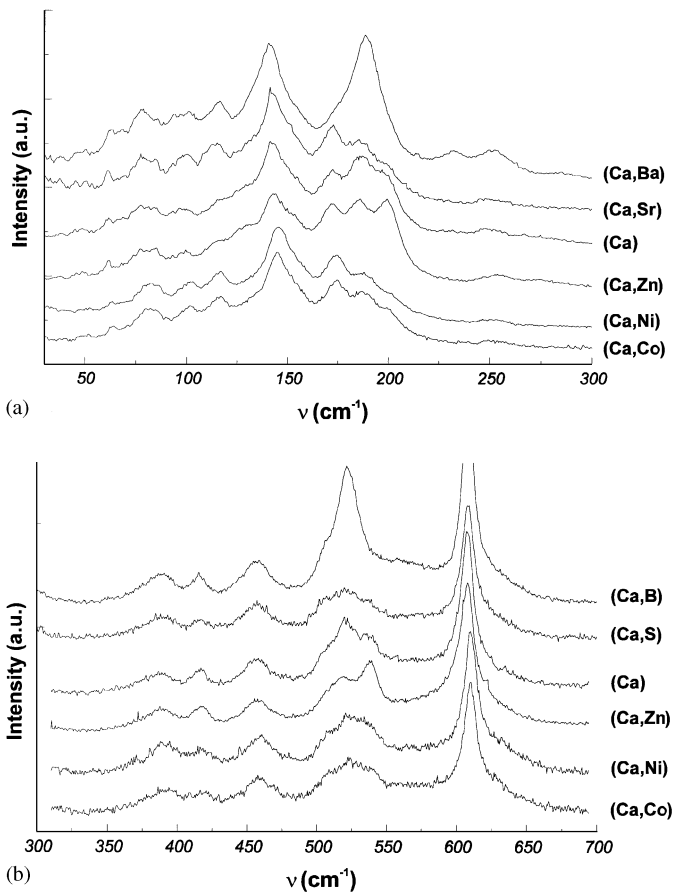

FIG. 4. Raman spectra, obtained at room temperature, for pure and various doped calcium tartrate tetrahydrate. Top, 0–350 cm^{-1} zone; bottom, 300–700 cm^{-1} zone.

different dehydratation temperature and the different electric behavior.

Three types of differences are observed between the pure crystal and the transition metal-doped crystals: the shortening of the Ca–O bonds (Table 4), the torsion angles in the coordination polyhedron and tartrate ion, (Table 5) and the hydrogen bond scheme (Table 3). The first finding is related to the decrease of the occupancy factor of the Ca site. The second and third are related to the localization of the doping atom.

In order to determine the possible site of the doping atom, the holes in the crystal structure were studied using the VALMAP computer program (26). A hole located at $(0.792, \frac{1}{2}, \frac{1}{8})$ was the largest in doped compounds (Fig. 3). This indicates that interstitial substitution may explain these structural differences.

As the localization of the hydrogen atoms from X-ray diffraction could not be reliable, these results were confirmed by Raman scattering measurements (Fig. 4). The room-temperature Raman spectrum of the calcium compound in different polarizations was shown by Taylor, Lockwood, and Labbé (27). In discussing the observed Raman spectra of these compounds, it is useful to classify vibrations as follows:

The rotatory and translatory external modes and the longitudinal acoustic mode first member (LAM-1) ($\nu < 300\ \mathrm{cm}^{-1}$), which give information about the packing forces. Assignment of these lines to specific vibrational modes is problematic due to the considerable mixing of mode character. The four spectra show clear differences in the number of modes and in the position and width of peak

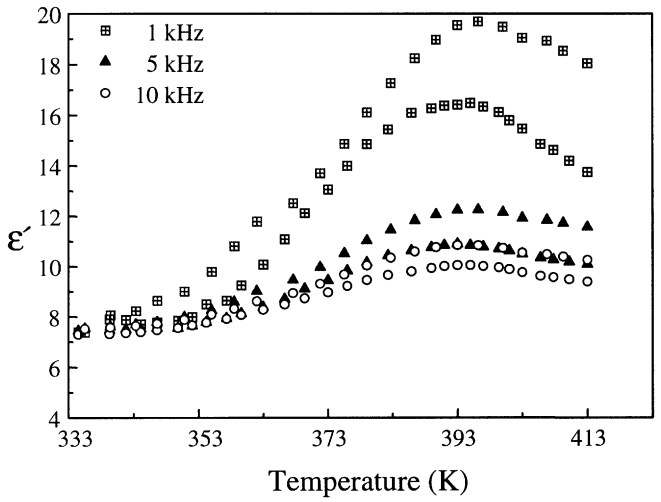

FIG. 5. Thermal dependence of dielectric permittivity real part at three frequencies. Upper values correspond to calcium tartrate doped with zinc, lower values to pure calcium tartrate. The rest of the doped compound shows a very similar behavior in which water loss occurs at upper temperatures.

TABLE 6
Temperature of Maximum Dielectric Permittivity Real Part at 1 kHz for Different Doped Crystals and Pure Calcium

	Temperature (in K) of maximum
Ca	396
Ca, Co	408
Ca, Zn	399
Ca, Sr	395
(Ca, Ba)	391

frequencies, particularly in the 116–121 mode and 171–200 cm^{-1} region. This suggests small differences in the crystal packing, confirming the results obtained from single-crystal X-ray diffraction.

The lattice and coordinated water molecules, librational modes ($300 < \nu < 600\ \mathrm{cm}^{-1}$). The molecular vibrations of the H_2O mloecule are well known (28–31). The differences are small with the exception of the $\rho_w(H_2O)$ mode. This mode is located in Ca substitution doping compounds at 522.9(2) cm^{-1} in Ba-doped and 523.5(5) cm^{-1} Sr-doped compounds. In interstitial doping compounds it is located at 528.7(4) cm^{-1} in Co-doped and 528.0(4) cm^{-1} in Ni-doped compounds and splits with different intensities at 512.6(6) and 535.2(8) cm^{-1} in Zn-doped compound. The values are 520.5(2) and 536.0(3) cm^{-1} for pure calcium tartrate tetrahydrate.

In the tartrate wagging/twisting mode zone ($1359 < \nu < 1500\ \mathrm{cm}^{-1}$) only a variation of the intensity of 1445.3 cm^{-1} band is observed for doped samples in interstitial sites. This mode is observed at 1443.0 cm^{-1} for the pure compound. No significant differences are observed in the rocking and stretching mode ($600 < \nu < 1350\ \mathrm{cm}^{-1}$) and HOH bending mode zones in interstitial doped compounds. The CO stretching mode splits at 1064–1070 cm^{-1} and 1150–1156 cm^{-1} in Ca substitution doped samples.

Dielectric permittivity temperature (Fig. 5) dependence shows qualitative differences between doped compounds and pure calcium tartrate tetrahydrate. The real part of permittivity increases in doped compounds. Table 6 shows the temperature where the real part of the permittivity is highest. The maximum was fitted assuming a Gaussian form for the peak. This temperature decreases when alkaline metals are used as doping atoms, which could be explained because the number of hydrogen bonds decreases when strontium and barium are used. The temperature increases when transition metal atoms are used which could be explained because the transition metal is coordinated with hydrated water molecules. Finally, the magnitude of dielectric permittivity increases when the surface molar fraction increases.

CONCLUSIONS

Different behavior is observed according to the doping atom. The doping atom substitutes Ca when an alkaline earth atom is used. The main structural differences are (1) the lengthening of the shortest Ca–O bonds and (2) the breaking of some of the hydrogen bonds which may be explained by an earlier water loss in this type of compound. The doping atom occupies an interstitial site when a transition metal atom is used. We found three types of structural differences: (1) the shortening of the shortest Ca–O bonds (the longest Ca–O bond remains constant), explained by the lowering of the occupancy factor in the Ca site; (2) torsion angles in tartrate ion; and (3) the hydrogen bond explained by the doping atom localization.

ACKNOWLEDGMENTS

C.G.-S. thanks the Consejería de Educación, Cultura y Deportes del Gobierno Autónomo de Canarias for financial support (No. 1999/061).

REFERENCES

1. C. C. Desai, A. H. Patel, and M. S. V. Ramana, *Ferroelectrics* **102,** 23 (1990).
2. M. M. Abdel-kader, F. El-Kabbany, S. Taha, A. M. Abosehly, K. K. Tahoon, and A. A. El-Sharkawy, *J. Phys. Chem. Solids* **52,** 655 (1991).
3. X. Solans, C. González-Silgo, and C. Ruiz-Pérez, *J. Solid State Chem.* **131,** 350 (1997).
4. Z. Brozek and K. Stadnicka, *Acta Crystallogr. B* **50,** 59 (1994).
5. A. C. Yanes, T. López, J. Stockel, J. F. Peraza, and M. E. Torres, *J. Mater. Sci.* **31,** 2683 (1996).
6. T. López, J. Stockel, J. F. Peraza, and M. E. Torres, *Cryst. Res. Technol.* **30,** 677 (1995).
7. F. C. Hawthorne, I. Borys, and R. B. Ferguson, *Acta Crystallogr. B* **38,** 2461 (1982).
8. H. B. Gon, *J. Crystal Growth* **102,** 501 (1990).
9. C. Ruiz-Pérez, M. Hernández-Molina, C. González-Silgo, X. Solans, T. López, and A. C. Yanes, *Acta Crystallogr. C* **52,** 2473 (1996).
10. C. K. Prout, J. R. Carruthers, and F. J. C. Rossoti, *J. Chem. Soc. A* 3336 (1971).
11. L. K. Templeton, D. H. Templeton, D. Zhang, and A. Zalkin, *Acta Crystallogr. C* **41,** 363 (1985).
12. C. González-Silgo, J. González-Platas, C. Ruiz-Pérez, T. López, and M. E. Torres, *Acta Crystallogr. C* **55,** 710 (1999).
13. M. E. Torres, T. López, J. Peraza, J. Stockel, A. C. Yánez, C. González-Silgo, C. Ruiz-Pérez, and C. P. Lorenzo-Luis, *J. Appl. Phys.* **84,** 5729 (1998).
14. C. González-Silgo, J. González-Platas, C. Ruiz-Pérez, T. López, and M. E. Torres, *Acta Crystallogr. C* **55,** 740 (1999).
15. G. K. Ambady, *Acta Crystallogr. B* **24,** 1548 (1968).
16. C. K. Fair, "MolEN. An Interactive Intelligent System for Crystal Structure Analysis." Enraf-Nonius, Delft, The Netherlands, 1990.
17. G. M. Sheldrick, "SHELXS, A computer program for crystal structure determination." Univ. Göttingen, Germany, 1997.
18. G. M. Sheldrick, "SHELXL, A computer program for crystal structure determination." Univ. Göttingen, Germany, 1997.
19. H. D. Flack, *Acta Crystallogr. A* **39**, 867 (1983).
20. M. E. Torres, Ph.D. Thesis, University of La Laguna, Spain, 1999.
21. M. E. Torres, J. Peraza, A. C. Yanes, X. Solans, E. Bocanegra, and C. Gonzalez-Silgo, *J. Phys. Chem. Solids*, in press.
22. A. R. Von Hippel, "Les diélectriques et leurs applications." Dunod, Paris, 1961.
23. J. Bohandy and J. C. Murphy, *Acta Crystallogr. B* **24,** 286 (1968).
24. S. C. Abrahams and E. T. Keve, *Acta Crystallogr. A* **27,** 157 (1971).
25. S. C. Abrahams, J. L. Bernstein, and E. T. Keve, *J. Appl. Crystallogr.* **4,** 284 (1971).
26. J. González-Platas, C. González-Silgo, and C. Ruiz Pérez, *J. Appl. Crystallogr.* **32,** 341 (1999).
27. W. Taylor, D. J. Lockwood, and H. J. Labbé, *J. Phys. C*: *Solid State Phys.* **17,** 1685 (1984).
28. G. Herzberg, "Infrared and Raman spectra of Polyatomic molecules." Van Nostrand, New York, 1945.
29. J. Bolard, *J. Chem. Phys.* **62,** 894 (1965).
30. J. Bolard, *J. Chem. Phys.* **62,** 900 (1965).
31. K. Nakamoto, "Infrared and Raman Spectra of Inorganic and Coordination Compounds," 4th Ed. Wiley, New York, 1986.